2-Deoxy-β-D-ribofuranosylamine: Quantum Mechanical Calculations of Molecular Structure and NMR Spin−Spin Coupling Constants in Nitrogen-Containing Saccharides

Francis Cloran,[†] Yuping Zhu,[†] John Osborn,[†] Ian Carmichael,*,[‡] and Anthony S. Serianni*,[†]

Contribution from the Department of Chemistry and Biochemistry and the Radiation Laboratory, University of Notre Dame, Notre Dame, Indiana 46556

*Received December 30, 1999. Revised Manuscript Received April 10, 2000*

Abstract: *Ab initio* molecular orbital (MO) and density functional theory (DFT) calculations using a polarized split-valence basis set have been performed on 2-deoxy-β-D-ribofuranosylamine (2-deoxy-β-D-*erythro*-pentofuranosylamine) in its unprotonated (**3**) and protonated (**4**) forms. Structural data confirm three previously reported factors influencing bond lengths in aldofuranosyl rings, and suggest the existence of a new 1,4-lone pair effect. Conformational energy profiles for **3** and **4** were compared to that described recently for 2-deoxy-β-D-ribofuranose (2-deoxy-β-D-*erythro*-pentofuranose) **5**. Results show that preferred conformation and energy barriers to pseudorotation are affected significantly by changes in C1 substitution. *N*-Protonation of **3** reduces pseudorotational barriers, suggesting a more flexible ring relative to the unprotonated molecule. NMR spin−spin coupling constants involving C1 and H1 were calculated in **3** and **4** using DFT methods described previously (Cloran *et al. J. Phys. Chem.* **1999,** *103,* 3783−3795). Trends in computed couplings as a function of ring conformation and C1 substitution confirm prior predictions based on experimental observations in aminosugars and nucleosides. In general, one- and two-bond J_{CH} and J_{CC} values appear more influenced by O → N substitution and by *N*-protonation than vicinal $^3J_{CH}$ and $^3J_{CC}$. These results will be useful in studies of related NMR scalar coupling constants in biologically relevant aminosugars and nucleosides, either free in solution or as components of oligosaccharides and oligonucleotides.

Introduction

It is well accepted that aldofuranosyl rings can exhibit considerable conformational flexibility in solution, either as free entities or as constituents of more complex biomolecules such as DNA and RNA.[1] This flexibility is commonly assumed to involve a two-state exchange between generalized North (N, ^{3}E) and South (S, ^{2}E) nonplanar conformers via a pseudorotational itinerary[2] (Scheme 1) or via inversion.[3] This two-state model derives mainly from studies of the biologically relevant β-D-*ribo* and 2-deoxy-β-D-*ribo* (2-deoxy-β-D-*erythro*-pento) rings and is often assumed to operate in aldofuranosyl rings having other structures and configurations. The latter assumption, however, is not strictly valid, especially since a complete understanding of the effects of furanose structure on ring conformation and dynamics remains elusive. Such an understanding would be valuable, since other ring configurations (e.g., α-D-*arabino*) and ring substitution patterns (e.g., glycosyl-amines) are encountered in biological systems.

Scheme 1

Pseudorotational itinerary of an aldofuranose ring
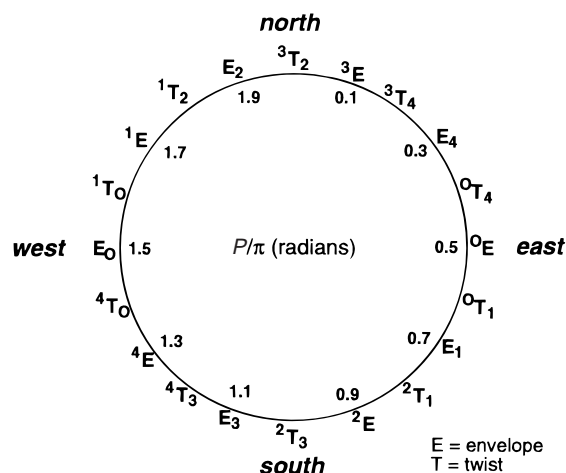
A key intermediate in the biosynthesis of purine ribonucleotides is β-D-ribofuranosylamine 5-phosphate **1**, the glycosylamine derived from β-D-ribofuranose 5-phosphate **2**.[4] The amino substituent at C1 of **1** might be expected to exert a significant effect on ring conformation, leading to different preferred conformations for **1** and **2**. This difference is anticipated because

* Address correspondence to this author.
† Department of Chemistry and Biochemistry.
‡ Radiation Laboratory.
(1) (a) Westhof, E.; Sundaralingam, M. *J. Am. Chem. Soc.* **1983,** *105,* 970−976. (b) Levitt, M.; Warshel, A. *J. Am. Chem. Soc.* **1978,** *100,* 2607−2613. (c) Westhof, E.; Sundaralingam, M. *J. Am. Chem. Soc.* **1980,** *102,* 1493−1500. (d) Olson, W. K. *J. Am. Chem. Soc.* **1982,** *104,* 278−286. (e) Olson, W. K.; Sussman, J. L. *J. Am. Chem. Soc.* **1982,** *104,* 270−278. (f) Harvey, S. C.; Prabhakaran, M. *J. Am. Chem. Soc.* **1986,** *108,* 6128−6136. (g) Pearlman, D. A.; Kim, S.-H. *J. Biomol. Struct. Dyn.* **1985,** *3,* 99−124.
(2) Altona, C.; Sundaralingam, M. *J. Am. Chem. Soc.* **1972,** *94,* 8205−8212.
(3) Westhof, E.; Sundaralingam, M. *J. Am. Chem. Soc.* **1983,** *105,* 970−976.
(4) Schendel, F. J.; Cheng, Y. S.; Otvos, J. D.; Wehrli, S.; Stubbe, J. *Biochemistry* **1988,** *27,* 2614−2623.

6436 *J. Am. Chem. Soc., Vol. 122, No. 27, 2000*

Cloran et al.

the anomeric effect,[5] which is a major factor dictating ring conformation in saccharides, differs in **1** and **2**, resulting in a modified interplay of competing structural forces. Given the small energy differences between the nonplanar conformers of **1** and **2**, any change in one structural factor is likely to alter preferred ring geometry.

In this report, the effect of amino group substitution at C1 of aldofuranosyl rings on ring structure and conformation has been investigated using ab initio molecular orbital (MO) and density functional theory (DFT) and a model aldopentofuranose, 2-deoxy-β-D-ribofuranosylamine (2-deoxy-β-D-*erythro*-pento-furanosylamine), in both its unprotonated (**3**) and protonated (**4**) forms. MO calculations were conducted on **3** as a function of the C1–N1 torsion angle, and the most stable geometry was compared to the most stable C1–O1 geometry observed in 2-deoxy-β-D-ribofuranose (2-deoxy-β-D-*erythro*-pentofuranose) **5**, which was studied previously using similar computational
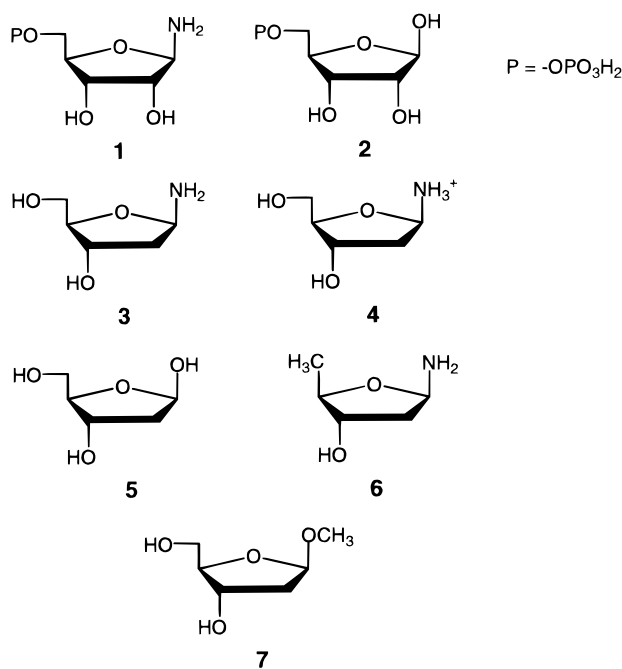
methods.[6,7] Comparisons between **3** and **4** were also made to evaluate the effect of *N*-protonation on ring structure and conformation. Finally, J_{CH} and J_{CC} values involving nuclei in the vicinity of C1 have been computed from DFT in **3** and **4** and compared to those computed previously in **5**,[7] yielding information on the effect of *N*-substitution and *N*-protonation on these couplings in saccharides. The latter results are compared to predictions made recently from studies of [^{13}C]-labeled aminosugars and nucleosides.[8,9] It should be noted that, while **3** and **4** are not strictly biologically relevant, they lack the C2,C3-diol fragment present in **1** which can complicate computational studies due to the possibility of differential intramolecular hydrogen bonding in some ring conformers. We elected to investigate **3** and **4** where this problem is absent

and the effects of *N*-substitution/protonation on furanose ring structure/conformation and NMR scalar couplings are more readily discerned.

Computational Methods

A. Geometry Optimization. Ab initio MO and DFT calculations were performed with a modified[10] version of the Gaussian 94 suite of programs.[11] For geometric optimization at the Hartree−Fock (HF) and DFT levels of theory, the polarized split-valence 6-31G* basis set[12] was employed. For DFT, the standard B3LYP functional, due to Becke,[13] was used in all calculations. This functional comprises both local[14] and nonlocal[15] exchange contributions and contains terms accounting for local[16] and nonlocal[17] correlation corrections.

As described for **5** previously,[6,7] the 10 envelope forms of **3** and **4** were examined by holding one endocyclic torsion angle fixed in each of 10 computations (i.e., for ^{3}E, the C4−O4−C1−C2 torsion was held constant at 0°). All remaining structural parameters were allowed to relax in each calculation unless otherwise noted. Individual envelope forms are identified throughout the paper via their corresponding pseudorotational phase angles,[2] *P* (Scheme 1), and are represented in graphical plots as *P*/π radians, where ^{3}E = 0.1 *P*/π (*P* = 18°), E$_4$ = 0.3 *P*/π (*P* = 54°), and so forth.

B. Calculations of NMR Spin−Spin Coupling Constants. ^{13}C−^{1}H and ^{13}C−^{13}C NMR spin−spin coupling constants in the DFT-optimized structures were obtained by finite-field (Fermi-contact) double perturbation theory[18] calculations at the B3LYP level using a basis set ([5s2p1d,2s]) previously constructed for similar systems.[10] Appropriate values for the perturbing fields imposed on the coupled nuclei were chosen to ensure sufficient numerical precision, while still allowing a satisfactory low-order finite-difference representation of the effect of the perturbation. Only the Fermi contact component of each coupling constant was considered due to the dominant relationship of this term in *J* values involving carbon and hydrogen, especially in saturated systems.

Results and Discussion

A. General Considerations. Initial calculations on **3** focused on the effect of C1−N1 bond rotation on conformational energy and structural parameters. Computations were conducted on the 10 envelope forms along the pseudorotational itinerary (Scheme 1). In all calculations, the same *initial* exocyclic torsion angles were chosen: H3−C3−O3−H, −60°; O4−C4−C5−O5, 60° (*gt* rotamer); and C4−C5−O5−H, 180°. The three initial C1−N1 rotamers in **3** are defined with respect to the orientation of the nitrogen lone pair as follows (Scheme 2): *gg*, lone pair gauche to O4 and C2; *gt*, lone pair gauche to O4 and trans to C2; and *tg*, lone pair trans to O4 and gauche to C2. Geometric optimizations were conducted with the 6-31G* basis set at the Hartree−Fock level of theory (HF/6-31G*).

During geometric optimizations of the E$_0$ and ^{1}E (1.5 and 1.7 *P*/π) ring forms of **3** in the *gt* rotamer, spontaneous bond

(5) Albright, T. A.; Burdett, J. K.; Whangbo, M.-H. *Orbital Interactions in Chemistry*; John Wiley and Sons: New York, 1985; pp 179−182.
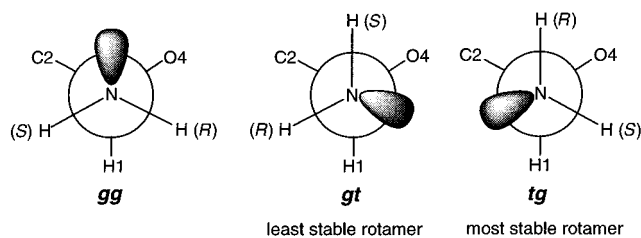(6) Church, T. J.; Carmichael, I.; Serianni, A. S. *J. Am. Chem. Soc.* **1997**, *119*, 8946−8964.
(7) Cloran, F.; Carmichael, I.; Serianni, A. S. *J. Phys. Chem.* **1999**, *103*, 3783−3795.
(8) Bandyopadhyay, T.; Wu, J.; Serianni, A. S. *J. Org. Chem.* **1993**, *58*, 5513−5517.
(9) Bandyopadhyay, T.; Wu, J.; Stripe, W. A.; Carmichael, I.; Serianni, A. S. *J. Am. Chem. Soc.* **1997**, *119*, 1737−1744.

(10) Carmichael, I. *J. Phys. Chem.* **1993**, *97*, 1789−1792.
(11) Frisch, M. J.; Trucks, G. W.; Schlegel, H. B.; Gill, P. M. W.; Johnson, B. G.; Robb, M. A.; Cheeseman, J. R.; Keith, T.; Petersson, G. A.; Montgomery, J. A.; Raghavachari, K.; Al-Laham, M. A.; Zakrzewski, V. G.; Ortiz, J. V.; Foresman, J. B.; Peng, C. Y.; Ayala, P. Y.; Chen, W.; Wong, M. W.; Andres, J. L.; Replogle, E. S.; Gomperts, R.; Martin, R. L.; Fox, D. J.; Binkley, J. S.; Defrees, D. J.; Baker, J.; Stewart, J. P.; Head-Gordon, M.; Gonzalez, C.; Pople, J. A. *Gaussian 94*; Gaussian, Inc.: Pittsburgh, PA, 1995.
(12) Hehre, W. J.; Ditchfield, R.; Pople, J. A. *J. Chem. Phys.* **1972**, *56*, 2257−2261.
(13) Becke, A. D. *J. Chem. Phys.* **1993**, *98*, 5648−5652.
(14) Slater, J. C. *The Self-Consistent Field for Molecules and Solids*; McGraw-Hill: New York, 1974.
(15) Becke, A. D. *ACS Symp. Ser.* **1989**, *394*, 165.
(16) Vosko, S. H.; Wilk, L.; Nusair, M. *Can. J. Phys.* **1980**, *58*, 1200.
(17) Lee, C.; Yang, W.; Parr, R. G. *Phys. Rev. B* **1988**, *37*, 785.
(18) Kowalewski, J.; Laaksonen, A.; Roos, B.; Siegbahn, P. *J. Chem. Phys.* **1979**, *71*, 2896−2902.

2-Deoxy-β-D-ribofuranosylamine

J. Am. Chem. Soc., Vol. 122, No. 27, 2000 6437

Scheme 2

gg

gt

least stable rotamer

tg

most stable rotamer

Figure 1. Conformational energy profiles for **3** (HF/6-31G*) as a function of the C1−N1 torsion angle (Scheme 1): open squares, *gg* rotamer; closed squares, *gt* rotamer; closed circles, *tg* rotamer.

rotations occurred to yield final structures significantly different from starting structures. For E_0, ring puckering changed to the ^0E form, whereas for ^1E, the C1−N1 bond torsion changed to the more stable *tg* rotamer. These rotations were considered undesirable since they, if uncorrected, would lead to structural and conformational energy comparisons between significantly different structures. Consequently, in these two cases, an additional structural constraint was added to the calculation (for E_0, the C4−O4−C1−C2 torsion angle was fixed at 28°; for ^1E, the O4−C1−N1−H*R* torsion angle was fixed at 207.7°). These torsions were chosen based on observed trends in these parameters in the remaining eight ring forms where geometric optimization proceeded smoothly. Therefore, molecular parameters calculated for the E_0 and ^1E forms of **3** (*gt* rotamer) contain more error, and may account for the small discontinuities observed in some of the plots of these parameters as a function of *P* for this structure.

The above HF/6-31G* calculations on **3** yielded a lowest energy structure with respect to C1−N1 torsion angle (*tg* rotamer, Scheme 2). The 10 envelope forms of **3** containing this C1−N1 torsion (denoted **3***tg*) were then geometrically reoptimized using DFT (B3LYP functional) and the 6-31G* basis set. This reoptimization was conducted to permit structural comparisons between **3***tg*, **4**, and **5**; similar DFT data on **4** were obtained in this study (see below), and DFT data on **5** were reported previously.[7] More importantly, however, the DFT-optimized geometries for **3***tg*, **4**, and **5** were required for calculations of J_{CH} and J_{CC} spin−spin coupling constants, since recent work has shown[7,19] that accurate couplings (less than 10% error) can be obtained using both DFT(B3LYP)/6-31G* geometries and DFT combined with finite-field perturbation theory and a specially designed basis set[10] without the need for scaling.

The symmetry of the NH_3^+ group in **4** eliminated the need for exploration of C1−N1 rotamers as required in **3**. Initial exocyclic torsions in **4** were identical to those used for **3**: H3−C3−O3−H, −60°; O4−C4−C5−O5, 60° (*gt* rotamer); and C4−C5−O5−H, 180°. Seven of the 10 envelope forms converged smoothly at the DFT(B3LYP)/6-31G* level of theory without large excursions in these torsions. In three geometries (E_3, ^4E, E_0), however, spontaneous rotation about the C4−C5 bond was observed, yielding the *gg* geometry (O5 gauche to O4 and C3); this rotation was apparently driven by H-bonding between the substituents on C1 and C5. For reasons discussed above, this rotation was prevented by holding the C3−C4−C5−O5 torsion angle constant at 180° in these structures. This additional structural constraint may introduce small deviations in bond lengths, angles, and torsions, and possibly lead to small discontinuities in graphical plots of the data for these forms.

B. Effect of the C1−N1 Torsion Angle on the Conformational Energies and Structural Parameters of 3. In aldofuranoses such as **5**, the preferred C1−O1 bond conformation can be predicted from a wealth of experimental and theoretical data
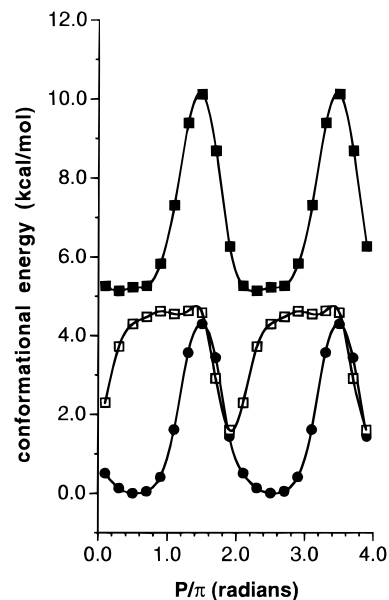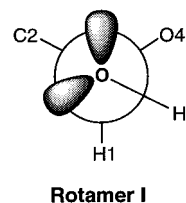
in the literature; the preferred geometry orients OH1 gauche to O4 and H1 (Rotamer I) due to the exoanomeric effect.[20−22] The

Rotamer I

situation is less clear for aldofuranosylamines such as **3**. Therefore, we examined the conformational energy of **3** as a function of pseudorotation phase angle (*P*) in the three staggered C1−N1 rotamers shown in Scheme 2. Three energy profiles were obtained (Figure 1), with the highest energy structures having the *gt* conformation (nitrogen lone pair trans to C2; defined hereafter as **3***gt*) and the lowest energy structures having the *tg* conformation (nitrogen lone pair trans to O4; defined hereafter as **3***tg*). The energy profiles for **3***gt* and **3***tg* are identical in shape and nearly identical in amplitude, with minimal energy structures located near ^0E (broad minimum) and the maximal energy structure located at E_0 (relatively sharp maximum). In contrast, the conformational energy profile for **3***gg* (nitrogen lone pair trans to H1) is shallower in amplitude and contains a broad maximum near $^2E/E_3$ and a sharp minimum at E_2. Thus, the effect of C1−N1 bond rotation on the conformational energy of **3** is significant. Stereoelectronic factors appear to explain the lowest energy structure (**3***tg*); the nitrogen lone pair, n_N, is closer in energy to $\sigma_{C1,O4}*$ than to $\sigma_{C1,H1}*$ and $\sigma_{C1,C2}*$, so that the $(n_N−\sigma_{C1,O4}*)$ interaction is favored over the $(n_N−\sigma_{C1,H1}*)$ and $(n_N−\sigma_{C1,C2}*)$ interactions. Similar arguments have been invoked to explain the preferred C1−O1 orientation and torsion in *O*-glycosides.[5]

It is interesting to note that the conformational energy profiles for **3***tg* and **3***gt* are virtually identical, with the latter profile shifted upward in energy by ~5 kcal/mol. Thus, despite the

(19) Cloran, F.; Carmichael, I.; Serianni, A. S. *J. Am. Chem. Soc.* **1999**, *121*, 9843- 9851.

(20) Lemieux, R. U.; Koto, S. *Tetrahedron* **1974**, *30*, 1933−1944.
(21) Praly, J.-P.; Lemieux, R. U. *Can. J. Chem.* **1987**, *65*, 213−223.
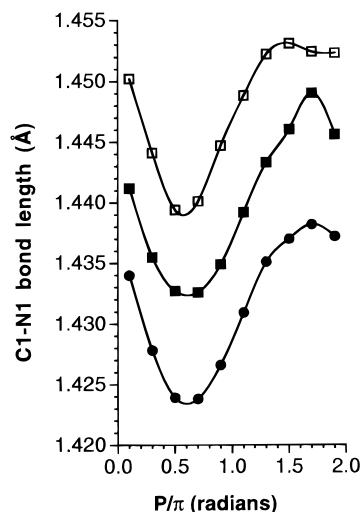(22) Lemieux, R. U. *Pure Appl. Chem.* **1971**, *25*, 527−548.

Figure 2. Effect of ring conformation on the C1−N1 bond length in **3** (HF/6-31G*) for the three C1−N1 rotamers (Scheme 1): open squares, *gg* rotamer; closed squares, *gt* rotamer; closed circles, *tg* rotamer.
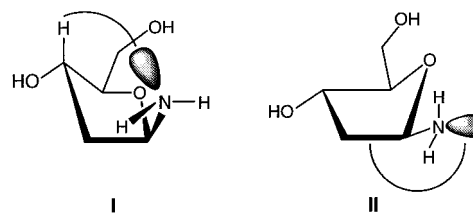
presence of the 1,3-interaction between the lone pairs at N1 and O4 in the $^0E/E_1$ geometries of **3***gt* these ring forms remain the most stable.

The most favored ring conformations of **3** lie in the eastern half of the pseudorotational itinerary, with the $^0E/E_1$ forms being lowest in energy. In these conformations, the C1−N1 bond is quasi-equatorial. As shown in Figure 2, this bond responds to ring conformation in a similar fashion in each of the three C1−N1 rotamers, with minimal bond length found when the C1−N1 bond is quasi-equatorial (near ^0E) and maximal bond length found when this bond is quasi-axial (near E_0). In any given ring conformation, the C1−N1 bond is shortest in the most stable *tg* rotamer.

Brameld and Goddard[23] reported recently the potential energies of **6** as a function of C1−N1 torsion angle and ring conformation based on MO calculations similar to those conducted here. The energy profiles for **6** are virtually identical to those found for **3**, suggesting that substitution at C4 of CH_3 for CH_2OH (when the latter assumes the *gt* conformation) exerts minimal effects on ring energies. The latter result accrues presumably because, in the *gt* conformation, O5 points "away" from the ring and is thus less likely to interact with ring substituents. On the other hand, a close correspondence would not be expected between **6** and **3** when the latter contains other C4−C5 torsions (e.g., *gg* conformation), based on recent observations.[24]

C−H bond lengths in **3** exhibit essentially the same dependence on ring conformation in each of the C1−N1 rotamers, except for the C3−H3 bond (Figure 3). The slightly longer C1−H1 bond in **3***gg* can be explained by noting that, in this C1−N1 rotamer, the nitrogen lone pair is trans to H1 (Scheme 2), thereby leading to bond elongation analogous to effects caused by oxygen lone pairs.[25,26] The reduced C2−H2*R* and C2−H2*S* bond lengths in **3***tg* and **3***gg*, respectively, are attributed to the previously reported 1,3 lone pair effect, which results in C−H bond shortening;[27] for example, in **3***gg*, the nitrogen lone pair

(23) Brameld, K. A.; Goddard, W. A., III *J. Am. Chem. Soc.* **1999**, *121*, 985−993.

(24) Cloran, F.; Carmichael, I.; Serianni, A. S. Manuscript in preparation.

(25) Serianni, A. S.; Wu, J.; Carmichael, I. *J. Am. Chem. Soc.* **1995**, *117*, 8645−8650.

(26) Podlasek, C. A.; Stripe, W. A.; Carmichael, I.; Shang, M.; Basu, B.; Serianni, A. S. *J. Am. Chem. Soc.* **1996**, *118*, 1413−1425.

Scheme 3

and H2*S* experience 1,3-interactions along the itinerary which presumably cause the observed bond shortening. The C4−H4 bond length is unaffected by C1−N1 rotation.

The aberant behavior of the C3−H3 bond deserves comment. It is important to note that **3***gt* and **3***tg* exhibit similar behavior; **3***gg* deviates from the others (Figure 3). The former behavior is consistent with the expected dependence of this bond on orientation, that is, bond length is maximal when quasi-axial ($E_2/^3E$) and minimal when quasi-equatorial ($^2E/E_3$).[25] Thus, the behavior of **3***gg* is unusual, and interestingly, its behavior is similar to that observed previously in β-D-ribofuranose[26] and 2-deoxy-β-D-*erythro*-pentofuranose.[6,7] While this unexpected behavior was noted in previous studies, we could not provide a plausible explanation for it. The present data show that the C3−H3 bond length is *reduced* in N forms of **3***gg* (as opposed to the C3−H3 bond length being enhanced in S forms), that is, *in ring geometries containing the shortest distances between the nitrogen lone pair and H3*. Thus, in addition to bond orientation, vicinal lone pair effects, and 1,3 lone pair effects, *1,4 lone pair effects* appear to occur in these ring systems (**I**, Scheme 3) and, like the 1,3-effects, lead to *bond shortening*.

The C1−O4, C4−O4, and C3−O3 bond length dependencies on ring conformation are independent of C1−N1 torsion (Figure 4). In any given ring conformation, the C1−O4 bond is longest in the most stable *tg* conformer. In contrast, similar lengths are observed for the C3−O3 bond in **3***gg*, **3***gt*, and **3***tg*.

The C2−C3, C3−C4, and C4−C5 bond lengths in **3** are similar in magnitude and exhibit the same dependence on ring conformation in each C1−N1 rotamer (Figure 5). In contrast, the C1−C2 bond in **3***gt* is longer than that found for **3***gg* and **3***tg*, although all three C1−N1 rotamers display the same C1−C2 dependence on ring conformation. The enhanced C1−C2 bond in **3***gt* is caused by vicinal lone pair effects; in this rotamer, the nitrogen lone pair is trans to the C1−C2 bond, thus enhancing its length as expected (**II**, Scheme 3). The C4−C5 bond shows the expected dependence on ring conformation, being longest when quasi-axial (near ^4E) and shortest when quasi-equatorial (near E_4) in **3***gg*, **3***gt*, and **3***tg*.[6,7,26]

Other molecular parameters such as C4−O4−C1 bond angle, puckering amplitude (τ_m), and C3−O3 torsion are largely unaffected by the C1−N1 torsion angle in **3** (Figure 6). Small differences are observed in the C4−O4−C1 bond angle and τ_m in western conformers.

C. DFT Structural Parameters and Conformational Energies in the Most Stable Forms of 3 and 5. The conformational energy profiles for **3***tg* and **5** determined from DFT differ significantly (Figure 7A); note that the conformational energy profiles for **3** determined at the HF (Figure 1) and DFT levels of theory (Figure 7A) are very similar. In this comparison, the exocyclic C3−O3, C4−C5, and C5−O5 torsions are similar in the two structures, the C1−N1 bond in **3** is *tg*, and OH-1 in **5** is gauche to O4 and H1 (Rotamer I). In **3***tg*, the energy minimum lies near E_1 and the energy maximum lies near E_0. In contrast,

(27) Kennedy, J.; Wu, J.; Drew, K.; Carmichael, I.; Serianni, A. S. *J. Am. Chem. Soc.* **1997**, *119*, 8933−8945.
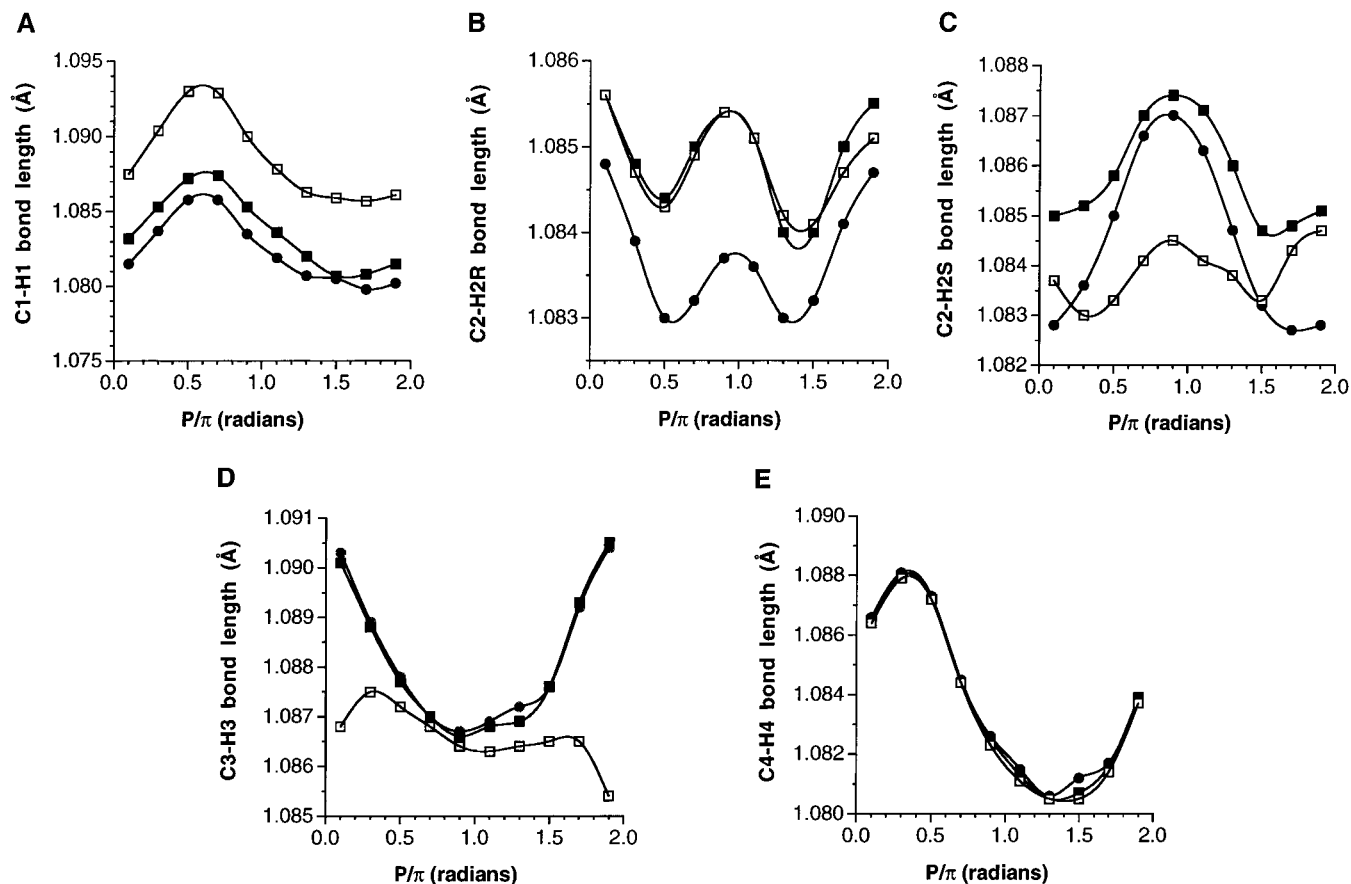
Figure 3. Effect of ring conformation on the C1−H1 (A), C2−H2*R* (B), C2−H2*S* (C), C3−H3 (D), and C4−H4 (E) bond lengths in **3** (HF/6-31G*) for the three C1−N1 rotamers (Scheme 2): open squares, *gg* rotamer; closed squares, *gt* rotamer; closed circles, *tg* rotamer.
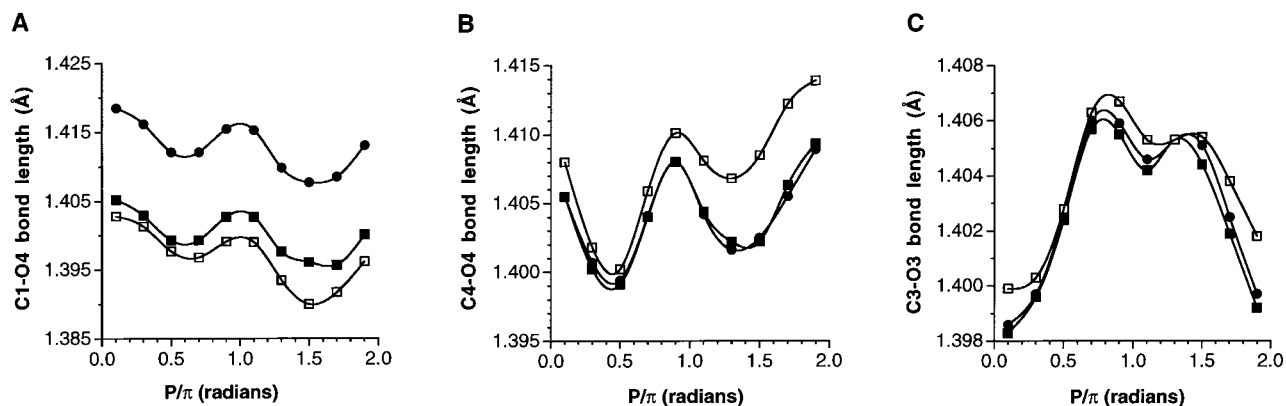

Figure 4. Effect of ring conformation on the C1−O4 (A), C4−O4 (B), and C3−O3 (C) bond lengths in **3** (HF/6-31G*) for the three C1−N1 rotamers (Scheme 2): open squares, *gg* rotamer; closed squares, *gt* rotamer; closed circles, *tg* rotamer.

for **5**, the energy minimum lies near E$_2$ and the energy maximum lies near ^{0}E. Thus, the preferred orientation of the C1−N1 and C1−O1 bonds in **3***tg* and **5**, respectively, differs, with the former preferring a quasi-equatorial orientation and the latter preferring a quasi-axial orientation. Both bonds, however, exhibit the same dependence on ring conformation (longest when quasi-axial (near E$_0$) and shortest when quasi-equatorial (near ^{0}E), although the C−N bond is longer in all ring conformations (Figure 8)).

The conformational energy profile for **3***gg* deviates significantly from those for **3***gt* and **3***tg* (Figure 1) but is similar to that observed for **5** (Figure 7A); for **3***gg* and **5**, the global minimum energy conformer is E$_2$. The loss of a lone pair trans to the C1−O4 bond in **3***gg* apparently eliminates the donor properties of N1 (see below), thereby allowing the donor

properties of O4 to dictate preferred conformation, as occurs in **5**. It is noteworthy that the conformational energy profile for **3***gt* is not the same as that for **5**, despite the lack of a lone pair trans to the C1−O4 bond. Thus, other factors must compete with the donor properties of O4 which favor geometries having the C1−N1 bond quasi-axial. Such factors may include the elongation of the C1−C2 bond (see below), which may stabilize geometries having the C1−N1 bond quasi-equatorial.

All C−H bonds in the furanose ring display the same dependence on ring conformation in **3***tg* and **5**, except for C3−H3 (Figure 9). The C1−H1 bond is uniformly shorter in **3***tg*, while the C2−H2*S* bond is uniformly longer. These effects may be attributed to vicinal[6,25,26] (C1−H1) and 1,3 lone pair[27] (C2−H2*S*) effects present in **5** but absent in **3***tg*. The behavior of
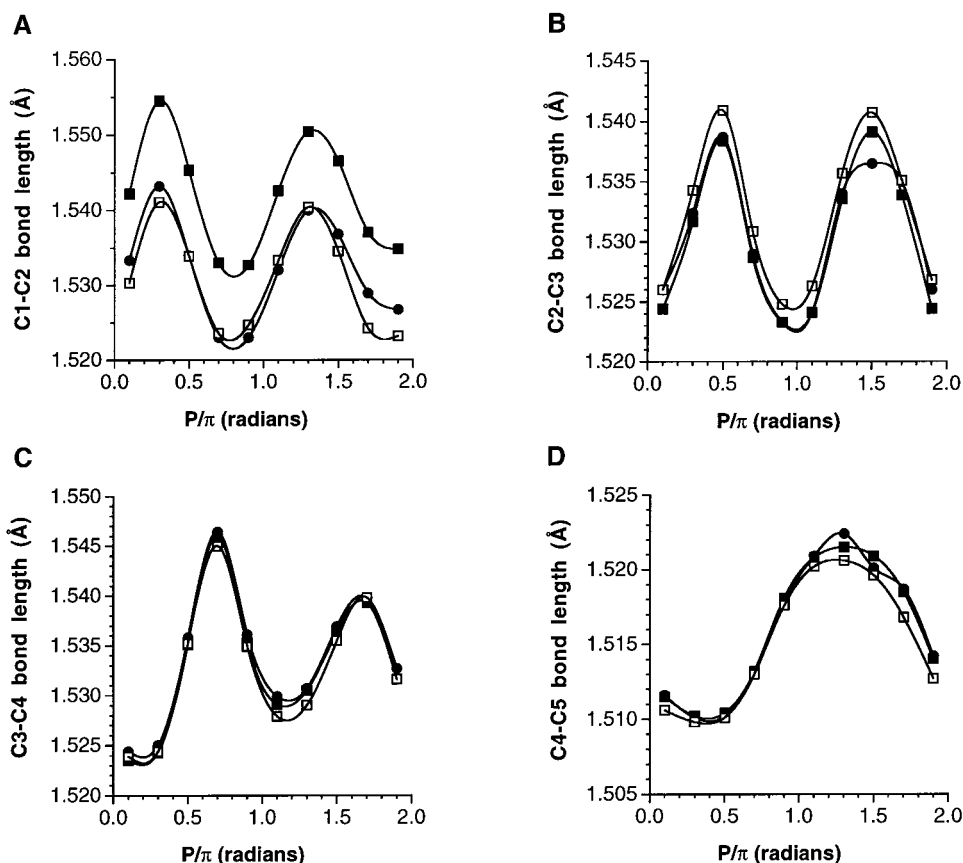
A

B

C

D

Figure 5. Effect of ring conformation on the C1−C2 (A), C2−C3 (B), C3−C5 (C), and C4−C5 (D) bond lengths in **3** (HF/6-31G*) for the three C1−N1 rotamers (Scheme 2): open squares, *gg* rotamer; closed squares, *gt* rotamer; closed circles, *tg* rotamer.
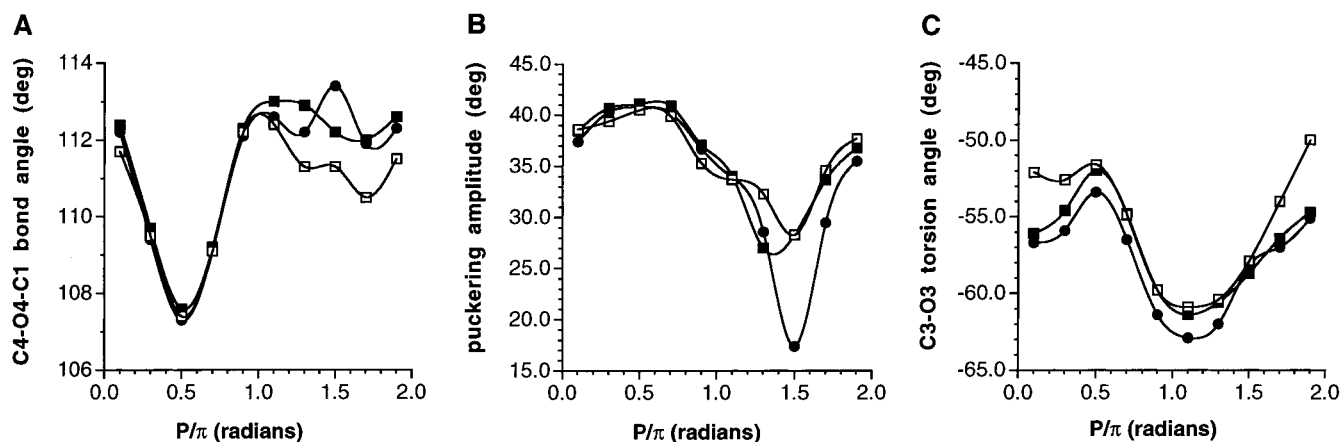
A

B

C

Figure 6. Effect of ring conformation on the C4−O4−C1 bond angle (A), puckering amplitude (τ_m) (B), and C3−O3 torsion angle (C) in **3** (HF/6-31G*) for the three C1−N1 rotamers (Scheme 2): open squares, *gg* rotamer; closed squares, *gt* rotamer; closed circles, *tg* rotamer. The τ_m value for E_o (*gt*) was fixed at 28° in the calculation (see General Considerations), thus leading to greater uncertainty in the resulting curve for western geometries.

C3−H3 confirms the existence of 1,4 lone pair effects discussed above. Calculations on **5** were conducted with the C1−O1 torsion orienting OH1 gauche to O4 and H1 (Rotamer I), and in this rotamer, one of the O1 lone pairs lies over the ring in N forms, thus reducing the C3−H3 bond length in these forms. The effect is absent in **3**tg, and thus the C3−H3 bond length increases in N forms as expected due to orientation factors (the bond is quasi-axial).

The C1−O4 bonds in **3**tg and **5** display similar dependencies on ring conformation, but this bond is uniformly longer in **3**tg (Figure 10A). The C3−O3 bond length is similar in **3**tg and **5** and displays a similar dependence on ring conformation.

Substitution of NH_2 for OH at C1 affects only the C1−C2 bond length, which is uniformly longer in **3**tg (Figure 11A). All other C−C bonds display similar lengths in **3**tg and **5**, and all C−C bonds show similar dependencies on ring conformation.

Minimal differences are observed in the C4−O4−C1 bond angle and C3−O3 torsion angle in **3**tg and **5**, although the former angles are moderately larger in the western forms of **3**tg (Figure 12).

D. Preferred Conformations of 3tg and 5 and Stereoelectronic Effects. The dissimilar conformational energy profiles of **3**tg and **5** (Figure 7A) suggest a different interplay of stereoelectronic factors at work in these compounds. This result
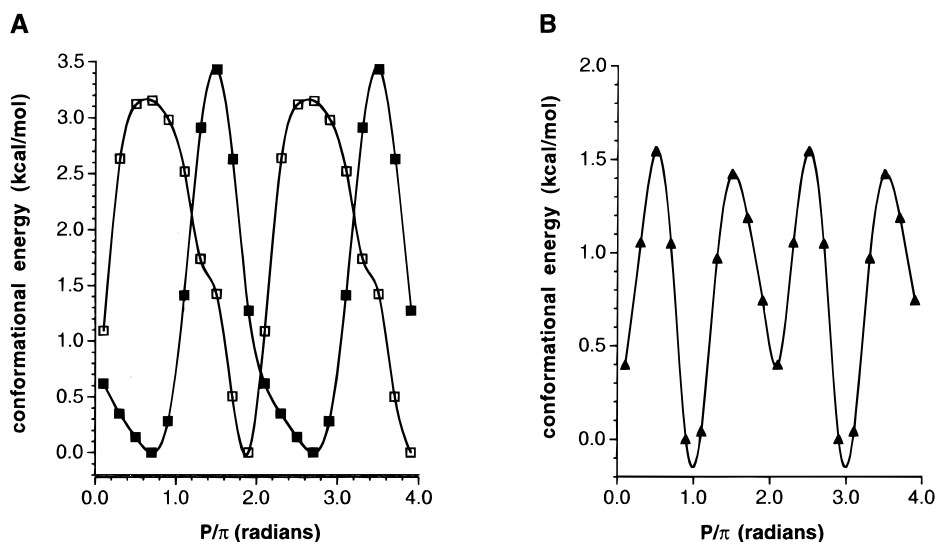
A

B

Figure 7. (A) Conformational energy profiles for **3** (DFT; B3LYP) in the *tg* rotamer (Scheme 2) and for **5** (DFT; B3LYP) in the C1−O1 rotamer shown in Rotamer I: closed squares, **3**; open squares, **5**. (B) Conformational energy profile for **4** (DFT; B3LYP).
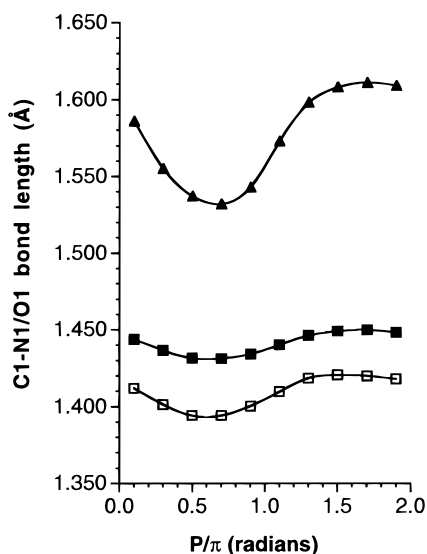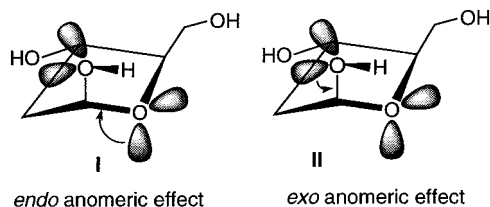

Figure 8. Effect of ring conformation on the C1−N1 or C1−O1 bond length in **3** (DFT; B3LYP) in the *tg* rotamer (Scheme 2), in **5** (DFT; B3LYP) in the C1−O1 rotamer shown in Rotamer I, and in **4**: closed squares, **3**; closed triangles, **4**. open squares, **5**.

Scheme 4

endo anomeric effect   *exo* anomeric effect

is expected, since in **3***tg*, dissimilar electronegative atoms are appended to the anomeric carbon, whereas in **5**, two oxygen atoms are involved. In **5**, the quasi-axial orientation of the C1−O1 bond in the preferred E2 conformer can be explained by invoking n$_O$ → σ$_{C1-O1}$* donation by the antiperiplanar O4 lone pair, causing the endocyclic C1−O4 bond to contract (Figure 10A) relative to the same bond in less stable ring forms (**I**, Scheme 4). This effect would cause the observed exocyclic C1−O1 bond elongation in E2 (Figure 8), although this lengthening may also be caused by general bond orientational factors in

Scheme 5

exo anomeric favored   *endo* and *exo* anomeric unfavored
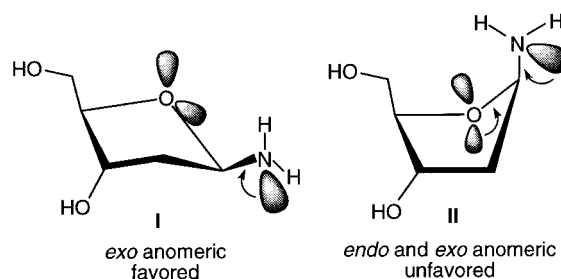
furanoses noted previously[25,26] (quasi-axial orientation favors longer bonds). Importantly, the C1−O1 bond elongation and the concomitant quasi-axial orientation are *reinforcing* factors. In the preferred E2 geometry, both *endo* (**I**, Scheme 4) and *exo* (**II**, Scheme 4) anomeric effects compete, but the *endo* effect appears to dominate. A dominant *exo* effect would favor a ring geometry having the C1−O1 bond quasi-equatorial (e.g., ^{2}E), since the resulting shorter C1−O1 bond would be better accommodated in this orientation.

In contrast, in **3***tg*, the *exo* anomeric effect appears to dominate. Thus, n$_N$ → σ$_{C1-O4}$* donation by the antiperiplanar N1 lone pair leads to a shortening of the exocyclic C1−N1 bond (Figure 8) and a lengthening of the endocyclic C1−O4 bond (Figure 10A) in the favored E1 conformer (**I**, Scheme 5). Both *endo* and *exo* anomeric effects potentially compete when the C1−N1 bond is quasi-axial (**II**, Scheme 5), but apparently this competition is avoided for the following reasons. It is well-known that nitrogen is a better donor than oxygen, and this preferred donor status results in a shortened C1−N1 bond, which is better accommodated in a furanose ring when quasi-equatorial than when quasi-axial. This latter orientational preference operates in concert with the dominant donor properties of nitrogen, leading to an avoidance of the potentially competing *endo* anomeric effect.

Regardless of whether the above stereoelectronic explanation of conformational preferences is correct, it is important to appreciate that the *N*-glycoside **3***tg* and the *O*-glycoside **5** prefer significantly different conformations, and that these differences may be important in biological processes involving these structures.

E. Effect of *N*-Protonation: Structural Comparisons between 3*tg* and 4. The conformational energy profile of **4**

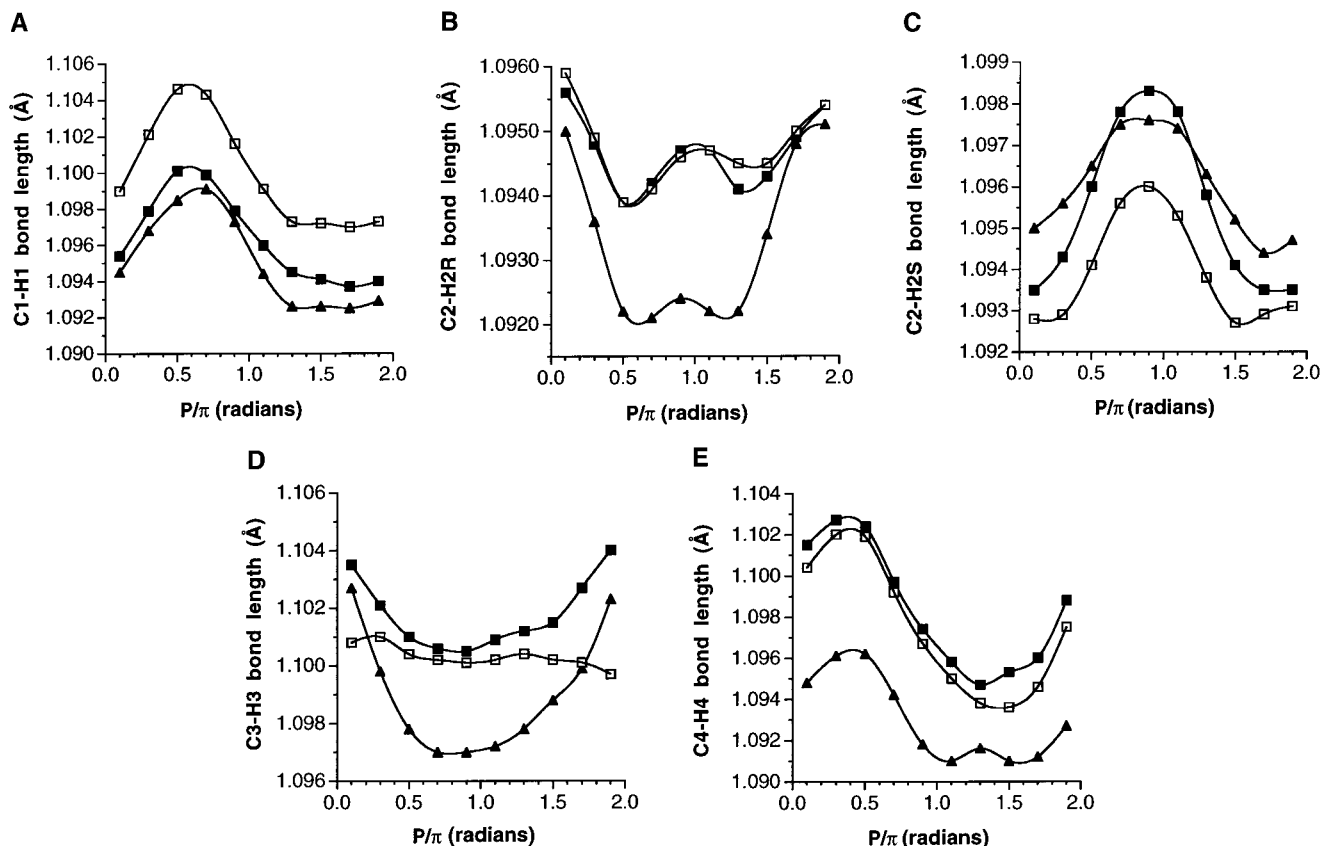**Figure 9.** Effect of ring conformation on the C1−H1 (A), C2−H2*R* (B), C2−H2*S* (C), C3−H3 (D), and C4−H4 (E) bond lengths in **3** (DFT; B3LYP) in the *tg* rotamer (Scheme 2), in **5** (DFT; B3LYP) in the C1−O1 rotamer shown in Rotamer I, and in **4**: closed squares, **3**; closed triangles, **4**; open squares, **5.**
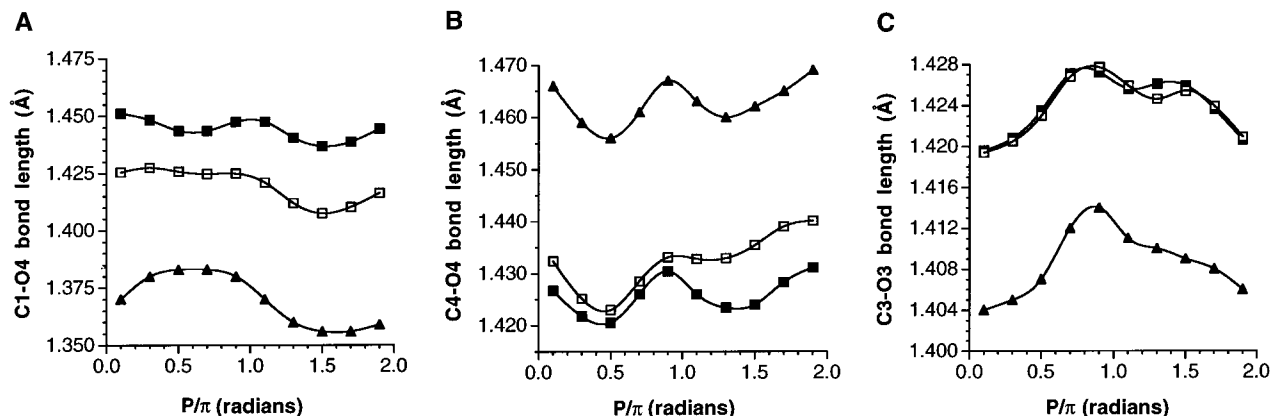

Figure 10. Effect of ring conformation on the C1−O4 (A), C4−O4 (B), and C3−O3 (C) bond lengths in **3** (DFT; B3LYP) in the *tg* rotamer (Scheme 2), in **5** (DFT; B3LYP) in the C1−O1 rotamer shown in Rotamer I, and in **4**: closed squares, **3**; closed triangles, **4**; open squares, **5.**

shows two well-defined minima at conformations near $^3T_2$ (North) and $^2T_3$ (South) (Figure 7B). This profile contrasts with those observed for **3***tg* and **5** in which only one well-defined energy minimum is observed (Figure 7A). Thus, *N*-protonation of **3***tg*, giving **4**, causes significant changes in preferred conformation; specifically, a small shift in the preferred S form occurs ($E_1 \rightarrow {}^2T_3$) and a new N energy minimum appears. The global minimum remains with S forms, but *N*-protonation confers stability to N geometries. Furthermore, the amplitude of the conformational energy curve for **4** (∼1.5 kcal/mol) is considerably smaller than that for **3***tg* (∼3.5 kcal/mol), suggesting greater conformational mobility in the protonated structure.

Differences in preferred ring geometry between **3***tg* and **4** must be associated, in part, with differences in stereoelectronic

properties. The appearance of a $^3T_2$ (north) minimum for **4** may be attributed to the loss of the *exo* anomeric effect arising from N1 (due to the unavailable nitrogen lone pair), resulting in domination by the *endo* anomeric effect exerted by O4. The latter effect favors a quasi-axial, or near quasi-axial, orientation of the C1−N1 bond as found in $^3T_2$. This situation is similar to that observed in **5**, which favors a north (E_2) geometry. However, despite this effect, south forms are still preferred over north forms of **4**, and this preference may arise, at least in part, to the increased steric bulk of the NH_3^+ group (relative to NH_2), which would favor the quasi-equatorial orientation of the C1−N1 bond found in $^2T_3$. Alternatively, the quasi-equatorial orientation of the C1−N1 bond in **4** may be stabilized relative to the quasi-axial orientation due to the reduced resultant dipole moment in the former.[28]
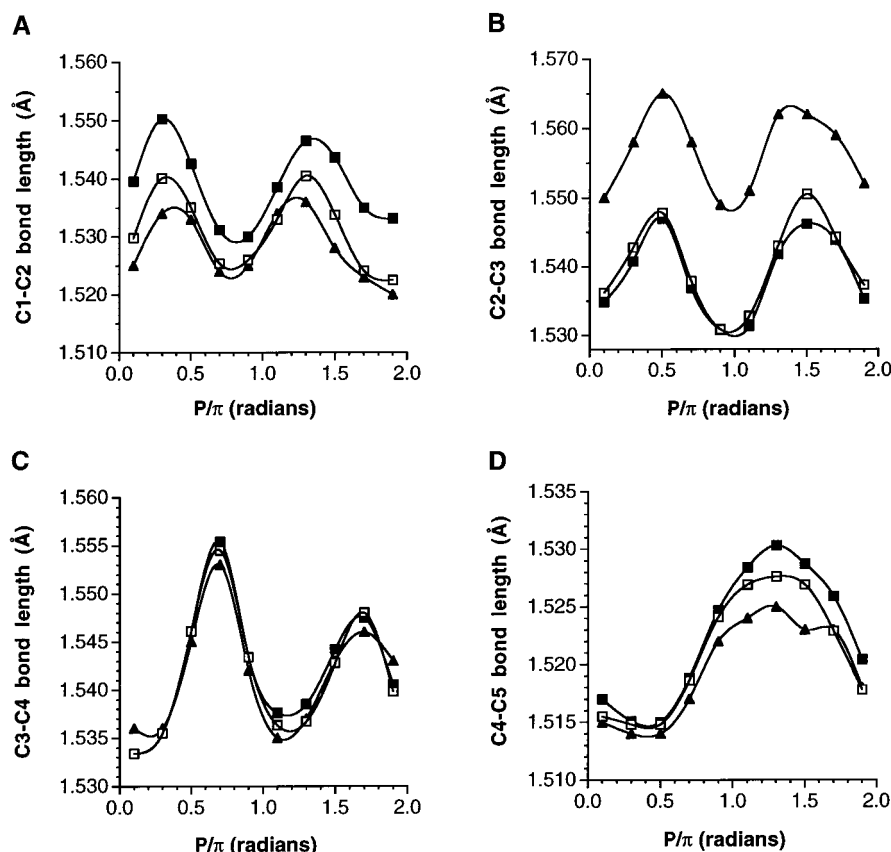
Figure 11. Effect of ring conformation on the C1−C2 (A), C2−C3 (B), C3−C4 (C), and C4−C5 (D) bond lengths in **3** (DFT; B3LYP) in the *tg* rotamer (Scheme 2), in **5** (DFT; B3LYP) in the C1−O1 rotamer shown in Rotamer I, and in **4**: closed squares, **3**; closed triangles, **4**; open squares, **5**.
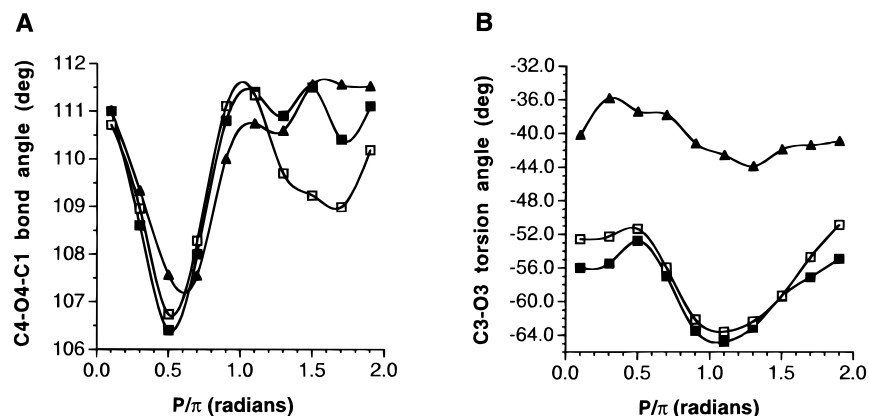

Figure 12. Effect of ring conformation on the C4−O4−C1 bond angle (A) and the C3−O3 torsion angle (B) in **3** (DFT; B3LYP) in the *tg* rotamer (Scheme 2), in **5** (DFT; B3LYP) in the C1−O1 rotamer shown in Rotamer I, and in **4**: closed squares, **3**; closed triangles, **4**; open squares, **5**.

N-Protonation causes substantial lengthening of the C1−N1 bond (Figure 8). This bond displays the same dependence on orientation as do the C1−N1 and C1−O1 bonds in **3***tg* and **5**,

(28) These results are consistent with complementary data obtained from DFT calculations on cyclohexanes and 2-substituted tetrahydropyrans bearing single CH₃, NH₂, NH₃⁺, and OH substituents. Energy differences, ($E_{eq} - E_{ax}$), where E_{eq} and E_{ax} are the computed total energies for a given substituent in equatorial and axial orientations, respectively, were found to be 2.2, 1.0, 1.2, and 0.4 kcal/mol for cyclohexane and 3.1, 2.5, 1.5, and −1.2 kcal/mol for 2-substituted tetrahydropyrans, for CH₃, NH₂, NH₃⁺, and OH, respectively. Thus, in cyclohexane, all four substituents prefer an equatorial orientation, with CH₃ and OH bracketing NH₂ and NH₃⁺. In contrast, only CH₃, NH₂, and NH₃⁺ prefer equatorial orientations in 2-substituted tetrahydropyrans, with OH preferring to be axial as expected. Importantly, NH₃⁺ displays a reduced preference for an equatorial orientation relative to NH₂, in agreement with the results obtained for the aldofuranosyl rings **3** and **4**.

respectively. Thus, the C1−N1 bond in **4** is shortest when quasi-equatorial (0.7 P/π; E₁) and longest when quasi-axial (1.7 P/π; ¹E). However, the *sensitivity* of the C1−N1 bond length in **4** to orientation is greater than observed in **3***tg* and **5**; in the former, an overall change of ∼0.07 Å is observed, compared to the more modest ∼0.01 Å changes in the latter. The reason for the enhanced sensitivity in **4** is unclear.

The C1−H1 and C2−H2*S* bond lengths are essentially unaffected by *N*-protonation (Figure 9A,C). In contrast, the C2−H2*R*, C3−H3, and C4−H4 bonds are shorter in **4**. The overall dependence of these bonds on ring conformation is conserved in **3***tg* and **4**.

N-Protonation causes significant shortening of the endocyclic C1−O4 bond (∼ −0.075 Å) and lengthening of the endocyclic
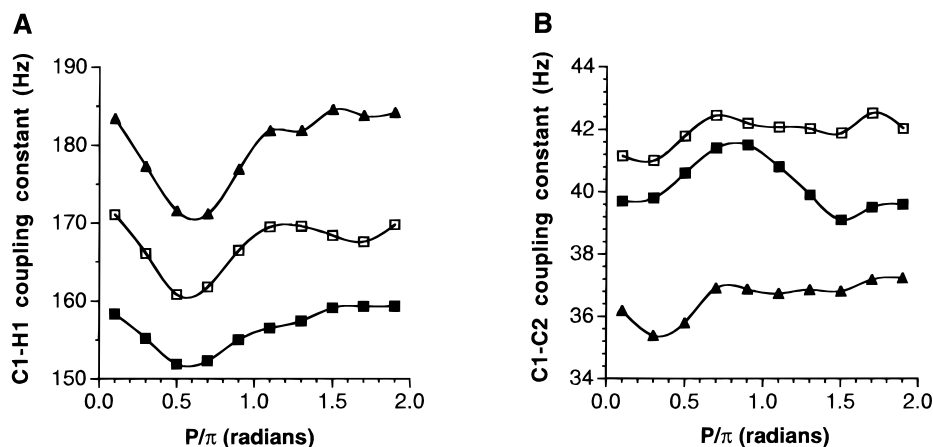
Figure 13. Effect of ring conformation on $^1J_{C1,H1}$ (A) and $^1J_{C1,C2}$ (B) in **3** (DFT; B3LYP) in the *tg* rotamer (Scheme 2) and in **5** (DFT; B3LYP) in the C1−O1 rotamer shown in Rotamer I: closed squares, **3**; closed triangles, **4**; open squares, **5**.

Figure 14. Effect of ring conformation on $^2J_{C1,H2R}$ (A), $^2J_{C1,H2S}$ (B), and $^2J_{C2,H1}$ (C) in **3** (DFT; B3LYP) in the *tg* rotamer (Scheme 2) and in **5** (DFT; B3LYP) in the C1−O1 rotamer shown in Rotamer I: closed squares, **3**; closed triangles, **4**; open squares, **5**.
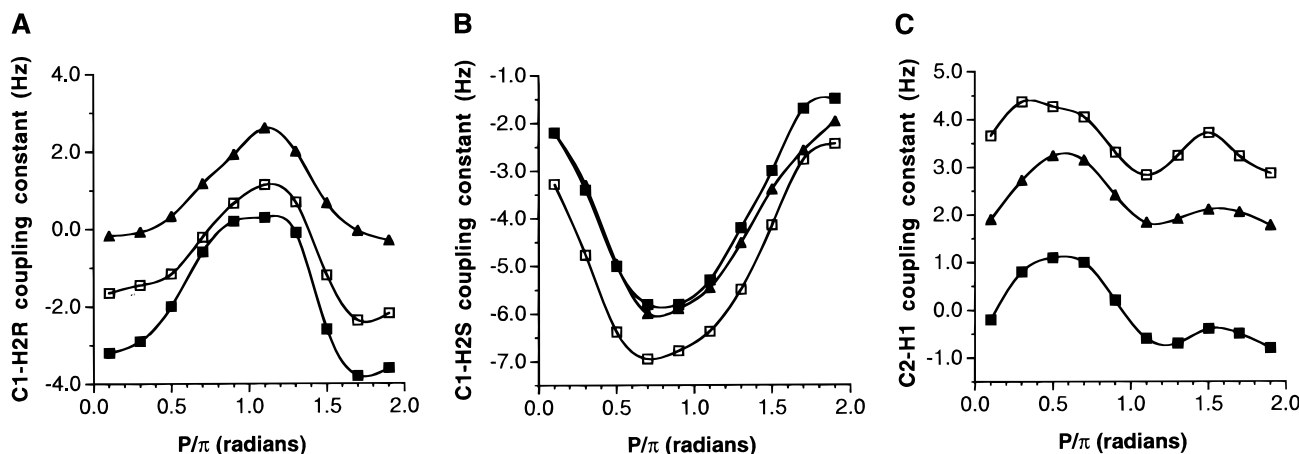
C4−O4 bond (∼ +0.04 Å) (Figure 10A,B). The exocyclic C3−O3 bond is shorter in **4** (∼ −0.02 Å) (Figure 10C) but the effect is reduced relative to the endocyclic C−O bonds, presumably because the bond is more remote from the site of protonation. The dependence of these bonds on ring conformation is conserved in **3***tg* and **4**.

The C1−C2 and C2−C3 bonds in **4** are shorter (∼ −0.01 Å) and longer (∼ +0.01 Å), respectively, than found for **3***tg*, whereas the C3−C4 bond is essentially unaffected (Figure 11A−C). The exocyclic C4−C5 bond appears unaffected by *N*-protonation in eastern conformers, but shortens in western forms (Figure 11D). The dependence of the C−C bonds on ring conformation is conserved in **3***tg* and **4**.

The C1−O4−C4 bond angle is essentially unaffected by *N*-protonation (Figure 12A). A more shallow C3−O3 torsion angle (∼ −40°) is observed in **4** relative to **3** (∼ −60°) (Figure 12B).

F. Calculated $^{13}C−^{1}H$ and $^{13}C−^{13}C$ Spin−Spin Coupling Constants in 3*tg*, 4, and 5. Computed J_{CH} and J_{CC} values were restricted to couplings involving the substituted carbon (C1) and its attached proton (H1) in **3***tg* and **4**, since the effect of O1 → N1 substitution on more remote coupling pathways was expected to be negligible. These couplings are compared to related values in **5**, which were reported previously.[7]

$^1J_{C1,H1}$ in **3***tg* is uniformly smaller than $^1J_{C1,H1}$ in **5** by ∼10 Hz (Figure 13A). However, $^1J_{C1,H1}$ in **3***tg* increases by ∼20 Hz upon *N*-protonation. In all compounds, $^1J_{C1,H1}$ exhibits the same dependence on ring conformation, although the magnitude of

change is not uniform (**3***tg* lowest, **4** highest). $^1J_{C1,C2}$ is also consistently smaller in **3***tg* than in **5**, although the difference is small (1−3 Hz) (Figure 13B); in contrast, $^1J_{C1,C2}$ is significantly reduced in **4** relative to **3***tg* and **5**. These results show that substitution of N1 for O1 affects $^1J_{CH}$ differently depending on the state of *N*-protonation, while $^1J_{C1,C2}$ is reduced upon *N*-substitution, with a greater effect observed for the protonated species. These results are consistent with recent comparisons of experimental $^1J_{CH}$ and $^1J_{CC}$ in methyl furanosides and nucleosides. For example, $^1J_{C1,H1}$ = 173.9 Hz in methyl 2-deoxy-β-D-*erythro*-pentofuranoside **7**[6] and $^1J_{C1',H1'}$ ranges from 167.4 to 170.8 Hz in 2′-deoxyribonucleosides.[8] $^1J_{C1,C2}$ = 40.5 Hz in **7** and $^1J_{C1',C2'}$ ranges from 36.6 to 37.2 Hz in 2′-deoxyribonucleosides.[9]

Two-bond $^{13}C−^{1}H$ couplings involving C1 and C2 were also calculated (Figure 14). Interestingly, OH1 → NH$_2$1 substitution exerts opposite effects on the magnitudes of $^2J_{C1,H2R}$ and $^2J_{C1,H2S}$, with the former showing a slightly reduced coupling and the latter showing a slightly enhanced coupling. In both cases, the effect is small (∼1 Hz), indicating that substitition of NH$_2$ for OH at the coupled carbon in a C−C−H pathway exerts a minor effect on $^2J_{CCH}$. These results are consistent with recent observations made in 2-acetamido-2-deoxy-glycopyranosides and in nucleosides.[9] The fact that opposite effects are observed, however, shows that both C−C−H pathways are not structurally equivalent, that is, the different orientations of electronegative substituents appended to these pathways yield different observed effects. *N*-Protonation does not appear to affect $^2J_{C1,H2S}$ signifi-
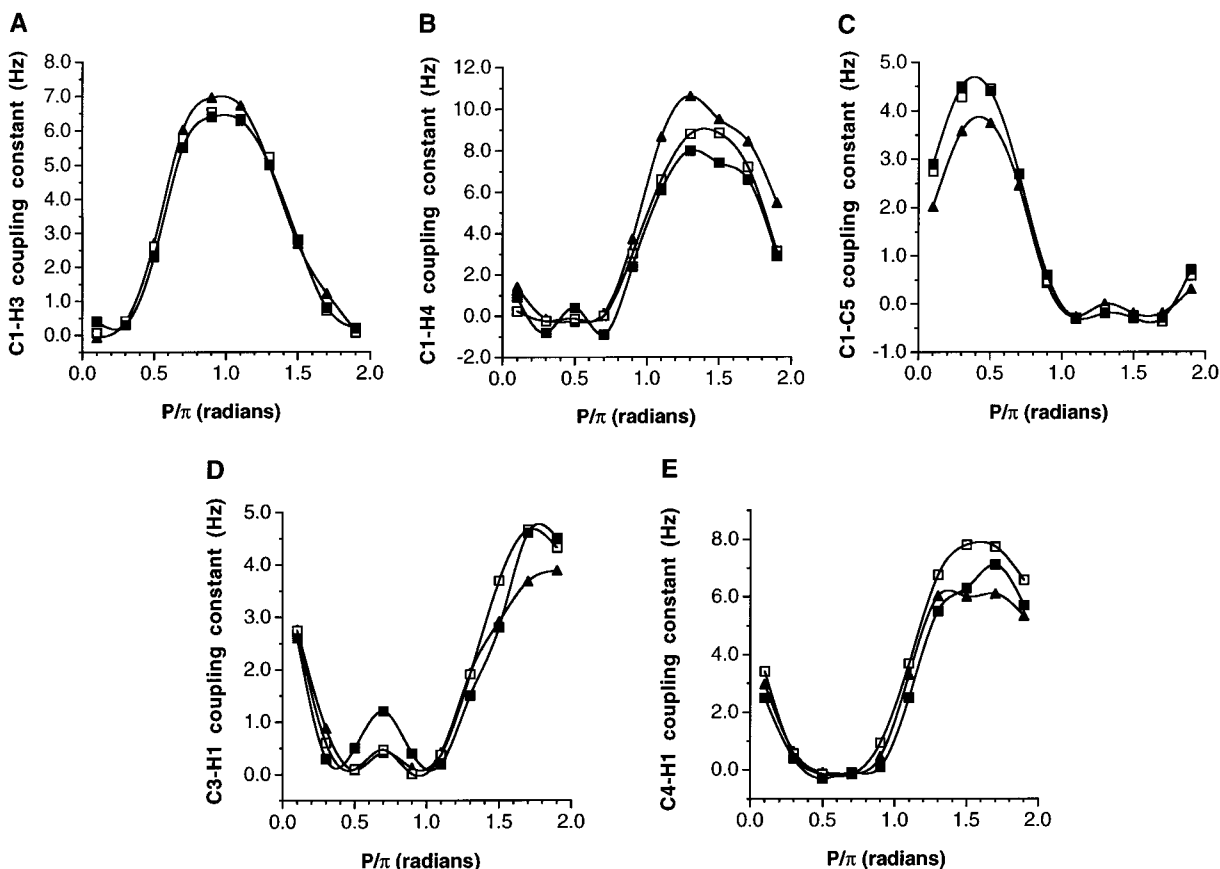
Figure 15. Effect of ring conformation on $^3J_{C1,H3}$ (A), $^3J_{C1,H4}$ (B), $^3J_{C1,C5}$ (C), $^3J_{C3,H1}$ (D), and $^3J_{C4,H1}$ (E) in **3** (DFT; B3LYP) in the *tg* rotamer (Scheme 2) and in **5** (DFT; B3LYP) in the C1–O1 rotamer shown in Rotamer I: closed squares, **3**; closed triangles, **4**; open squares, **5.**

Figure 16. Effect of ring conformation on $^{2+3}J_{C1,C3}$ (A) and $^{2+3}J_{C1,C4}$ (B) in **3** (DFT; B3LYP) in the *tg* rotamer (Scheme 2) and in **5** (DFT; B3LYP) in the C1–O1 rotamer shown in Rotamer I: closed squares, **3**; closed triangles, **4**; open squares, **5.**
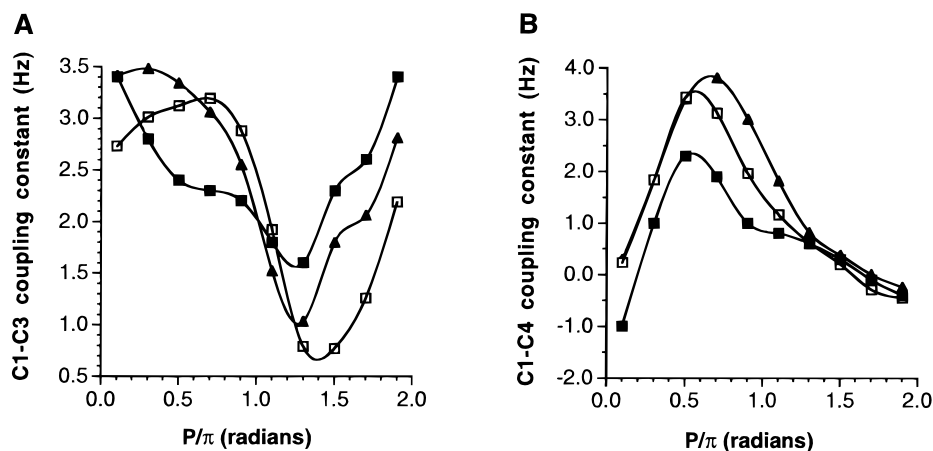
cantly, but $^2J_{C1,H2R}$ is shifted to a more positive value by ∼3 Hz; again, seemingly similar pathways manifest much different behaviors. In contrast, OH → NH$_2$ substitution at the carbon bearing the coupled proton causes a substantial decrease in $^2J_{CCH}$, as manifested in the different $^2J_{C2,H1}$ values calculated in **3***tg* and **5** (Figure 14C). This decrease (∼3.5 Hz) is in good agreement with earlier findings in 2-acetamido-2-deoxy-glyco-pyranosides and in nucleosides,[9] where a decrease of ∼2.5 Hz was estimated. Interestingly, this decrease is substantially reduced upon *N*-protonation (Figure 14C), resulting in more similar $^2J_{C2,H1}$ in **4** and **5**.

The vicinal couplings, $^3J_{C1,H3}$, $^3J_{C1,H4}$, $^3J_{C3,H1}$, and $^3J_{C4,H1}$, are virtually identical in **3***tg*, **4**, and **5**, indicating that *N*-substitution/protonation at the carbon bearing the coupled proton, or

substitution at the coupled carbon, influences $^3J_{CCCH}$ and $^3J_{COCH}$ minimally (Figure 15). $^3J_{C1,C5}$ values in **3***tg*, **4**, and **5** are also very similar.

Two dual-pathway ^{13}C–^{13}C couplings were examined, namely, $^{2+3}J_{C1,C3}$ and $^{2+3}J_{C1,C4}$ (Figure 16). The behavior of the latter is essentially the same in **3***tg*, **4**, and **5**; the more negative couplings in western forms (relative to eastern forms) have been explained previously.[7] These results suggest that *N*-substitution on $^2J_{COC}$ values will be small. $^{2+3}J_{C1,C3}$, however, displays significant differences in **3***tg* and **5**, and coupling along this pathway will be affected by the relative orientation of the terminal electronegative substituents. In **5**, both are oxygens, and thus coupling is similar (0.7 Hz difference) in the extreme geometries (^{2}E and E$_2$) where quasi-axial and quasi-equatorial orientations are

interchanged. These extreme geometries, however, do not yield equivalent couplings in **3***tg*, and a greater difference in coupling is observed (1.2 Hz). However, the coupling difference is still small, thus confirming recent predictions of the behavior of $^{2+3}J_{C1,C3}$ in ribonucleosides and 2′-deoxyribonucleosides.[9] The effect of ring conformation on $^{2+3}J_{C1,C3}$ in **4** is more similar to that observed for **5**, suggesting that NH_3^+ more closely mimics OH than does NH_2.

Conclusions

The structural and conformational properties of 2-deoxy-β-D-*erythro*-pentofuranosylamine in its unprotonated (**3**) and protonated (**4**) forms, as derived from molecular orbital calculations at the HF and DFT (B3LYP) levels of theory using the 6-31G* basis set, have been investigated in this report. These properties are compared to those reported previously for 2-deoxy-β-D-*erythro*-pentofuranose **5**.[6,7] Substitution of NH_2 or NH_3^+ for OH at the anomeric carbon of **5** and substitution of NH_3^+ for NH_2 at the anomeric carbon of **3** significantly affect the molecular structure and preferred conformation of the furanose ring. Furthermore, the effects of NH_2 and NH_3^+ substitution on J_{CH} and J_{CC} values involving nuclei in the vicinity of the anomeric carbon were examined to test previous predictions on the effect of O → N substitution in saccharides based on limited experimental observations.[8,9] This information will assist in future interpretations of J_{CH} and J_{CC} values in nucleosides, aminosugars, and other nitrogen-substituted saccharides.

Geometric optimizations conducted as a function of pseudorotational phase angle and C1−N1 bond torsion yielded three distinct conformational energy profiles for **3**, with the most stable C1−N1 rotamer orienting the nitrogen lone pair trans to O4. Three major factors affecting bond length in furanose rings, identified in previous investigations, are confirmed in **3** and summarized in Scheme 6: orientational factors (for exocyclic bonds; quasi-axial or quasi-equatorial), vicinal lone pair effects, and 1,3 lone pair effects. The present results for **3**, however, suggest that a fourth factor influences exocyclic bond lengths, namely, a 1,4 lone pair effect (Scheme 6). This factor explains the anomalous conformational dependence of the C3−H3 bond reported previously in 2-deoxy-β-D-*erythro*-tetrofuranose,[25,27] β-D-ribofuranose,[26] and 2-deoxy-β-D-*erythro*-pentofuranose.[6,7] The preferred C1−N1 rotamer in **3** (*tg*) prevents this interaction, and thus the C3−H3 bond in this compound behaves as expected. In **5**, however, the preferred C1−O1 rotamer (Rotamer I) places an oxygen lone pair in proper orientation to cause C3−H3 bond length truncation in N forms.

The significantly different preferred ring conformations of **3** and **5** determined with the most stable C1−O1/N1 rotamers can be explained by invoking stereoelectronic arguments involving lone pairs in the vicinity of the anomeric carbon. Competing *endo* and *exo* anomeric effects appear to dictate preferred conformation; in **5**, the *endo* effect dominates, whereas in **3**, the *exo* effect dominates. In both cases, the preferred orientation of the exocyclic C1−O1/N1 bond reinforces these interactions. In contrast, the *endo* effect of O4 dominates in **4**, thus stabilizing north forms, but south forms of **4** (in which the C1−N1 bond is quasi-equatorial) are still preferred, presumably due to the steric requirements of NH_3^+ and/or the reduced resultant dipole moment. It is noteworthy that stereoelectronic and other structural effects in saccharides can be studied conveniently in furanosyl rings due to their ability to assume a continuous range of nonplanar conformations in which all ring substituents are able to orient either quasi-axially or quasi-equatorially without
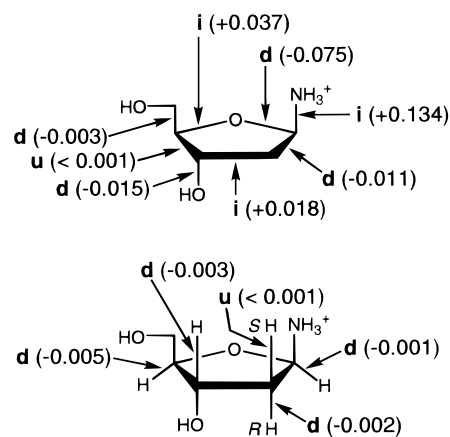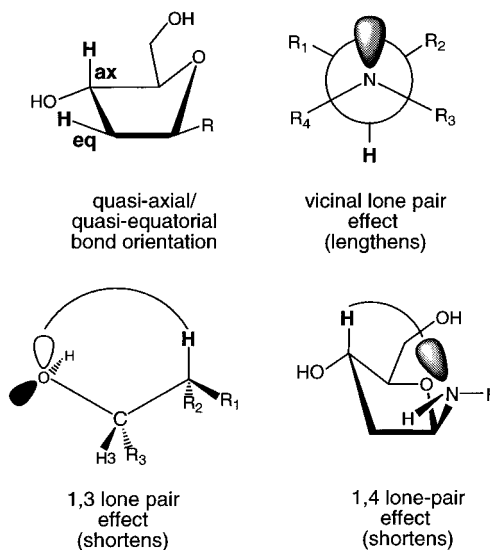

Figure 17. Changes in C−H, C−C, C−N, and C−O bond lengths (B3LYP/6-31G*) upon N1 protonation: d = decrease, i = increase, u = unchanged. Values in parentheses denote the average bond length change (in Å) over the pseudorotational itinerary.

Scheme 6

quasi-axial/
quasi-equatorial
bond orientation

vicinal lone pair
effect
(lengthens)

1,3 lone pair
effect
(shortens)

1,4 lone-pair
effect
(shortens)

the need to break bonds. For example, the C1−O1 bond can assume a quasi-axial or quasi-equatorial orientation in *relatively stable geometries* of **5**, whereas a similar transformation in aldopyranosyl rings is often very energetically unfavorable (e.g., $^4C_1/^1C_4$ interconversion). In the latter system, anomeric pairs are usually studied, necessitating comparisons between two different molecular structures.

The preferred quasi-equatorial orientation of the C1−N1 bond in **4** might be considered a manifestation of the reverse anomeric effect in saccharides,[29] were it not also true that the C1−N1 bond in **3** prefers the same orientation. Furthermore, *N*-protonation of **3**, giving **4**, results in increased stabilization of forms containing quasi-axial C1−N1 bonds, that is, protonation results in the stabilization of particular ring geometries via the normal *endo* anomeric effect. This effect can be rationalized from resonance considerations; hyperconjugative structures generated from C1−N1 bond breaking in **4** when the C1−N1 bond is quasi-axial do not suffer from charge separations, in contrast to a similar treatment in **3**, and thus anomeric effects in **4** would be expected to be at least as strong as those in **3**. These observations reinforce the view that reverse anomeric effects do not exist,[30] at least in structures such as **4**.

(29) (a) Lemieux, R. U.; Morgan, A. R. *Can. J. Chem.* **1965**, *43*, 2205−2213. (b) Lemieux, R. U. *Pure Appl. Chem.* **1971**, *25*, 527−548.
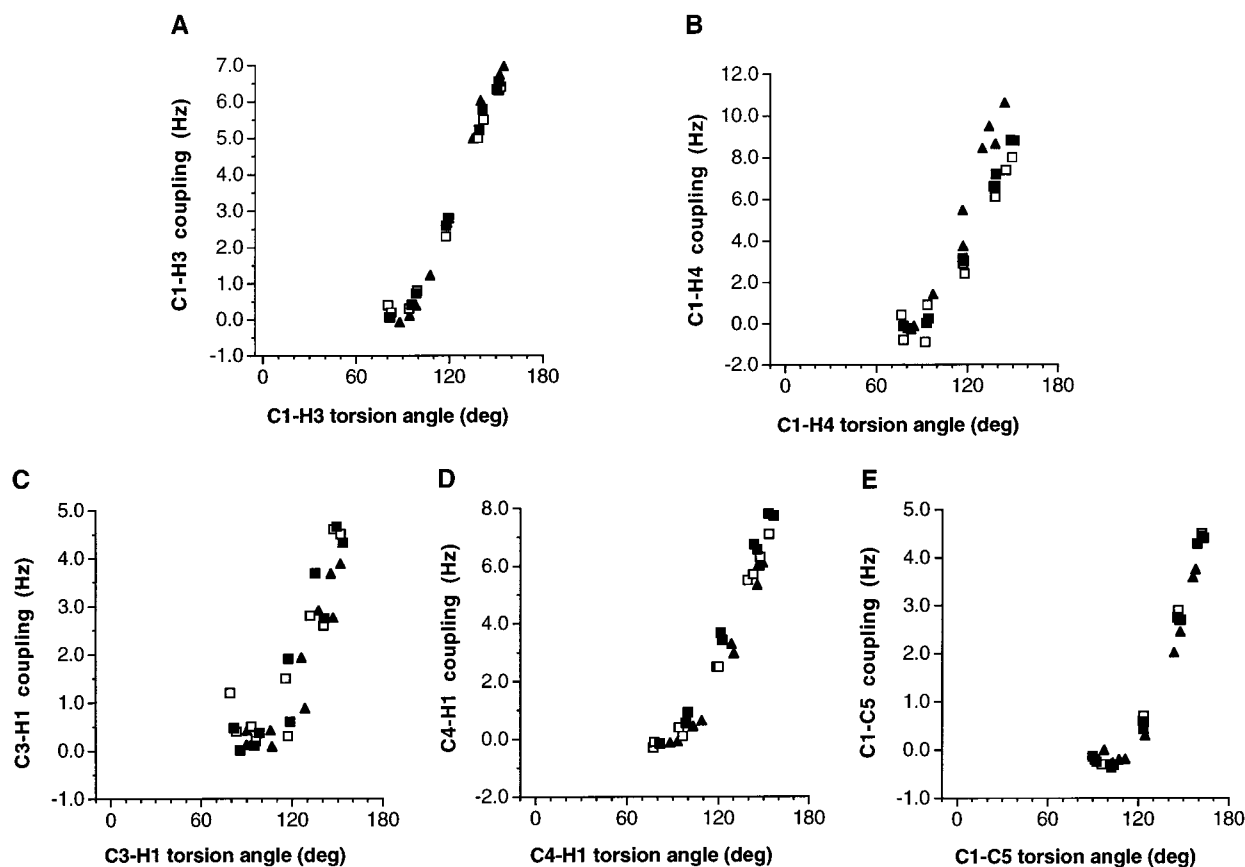
Figure 18. Calculated partial Karplus curves for specific $^3J_{CH}$ and $^3J_{CC}$ in **3***tg*, **4**, and **5**: (A) $^3J_{C1,H3}$, (B) $^3J_{C1,H4}$, (C) $^3J_{C3,H1}$, (D) $^3J_{C4,H1}$, (E) $^3J_{C1,C5}$; open squares, **3**; closed triangles, **4**; closed squares, **5**.

It should be appreciated that the stereoelectronic factors involving the anomeric carbon of **3** which influence ring conformation in this structure are not strictly transferable to nucleosides. In the former, a localized lone pair resides on N1, thereby permitting n → σ* donation, whereas in nucleosides, the lone pair is delocalized within the aromatic base, making this donation unlikely. This difference is important when considering stereoelectronic factors that control C1−N1 bond orientation and furanose ring conformation in nucleosides.

While the observation that **3** and **5** differ considerably in preferred conformation is important to appreciate, it should be recognized that the protonated form of glycofuranosylamines such as **1**, and not the unprotonated form, will dominate in solution under physiological conditions. The results of the present calculations show that N1 protonation exerts a major effect on furanose structure and conformational energy. Significant changes are observed in C−C, C−N, and C−O bond lengths, as summarized in Figure 17. Interestingly, changes in bond length appear to alternate systematically through the structure, i.e., increase → decrease → increase, etc. In contrast, C−H bond lengths remain relatively unchanged. N1 protonation also lowers the barrier to pseudorotation, suggesting more conformational flexibility, and appears to stabilize north (N) forms. A more conventional N/S conformational model therefore emerges for **4**, whereas only a single energy minimum is observed for **3**. Thus, protonation at the exocyclic N1 of **3** induces pervasive structural changes in the molecule reminiscent of those caused by furanose ring−oxygen protonation reported recently.[27] It should be appreciated that the protonation state of a molecule free in solution may not be the preferred state in an

enzyme active site; for example, in the conversion of 5-phosphoribosyl-α-pyrophosphate (PRPP) to **1** during the biosynthesis of inosine monophosphate (IMP), the initially formed **1** in the active site may be unprotonated, and only upon release to solution does protonation occur. The latter release may be accompanied by substantial changes in preferred furanose conformation and conformational dynamics (i.e., bound and free geometries may differ).

The observed effects of O1 → N1 substitution on computed J_{CH} and J_{CC} values are in very good agreement with prior predictions. Previous suggestions[9] that a different projection rule is required for the interpretation of $^2J_{C2,H1}$ in nucleosides are validated. The present results also explain why, for example, $^2J_{C1,H2R/S}$ and $^3J_{C1,H3}$ in *O*-glycoside models and nucleosides are in close agreement; present data show that O1 → N1 substitution exerts only a minor effect on their magnitudes. In general, $^3J_{CCCH}$, $^3J_{COCH}$, and $^3J_{COCC}$ are affected minimally by O → N substitution at terminal carbons, regardless of the state of *N*-protonation; this result is clearly depicted in Figure 18, which shows similar partial Karplus curves constructed from related $^3J_{CH}$ and $^3J_{CC}$ in **3***tg*, **4**, and **5**. In contrast, $^2J_{CCH}$ values are affected significantly when the substitution change occurs at the carbon bearing the coupled proton; a much smaller effect is observed when the substitution occurs at the coupled carbon.

The *J*-coupling/structure correlations drawn from this work lend themselves to systematic experimental validation. For example, $^1J_{C1,H1}$ and $^1J_{C1,C2}$ in **3** are predicted to increase by ∼10 Hz and decrease by ∼2−4 Hz, respectively, upon *N*-protonation. Thus, these one-bond couplings, especially $^1J_{C1,H1}$, might serve as useful probes of the state of protonation of amino-containing saccharides in solution. Two-bond $^{13}C−^1H$ spin-couplings in **3** are also affected by *N*-protonation, although like

(30) Perrin, C. L.; Armstrong, K. B. *J. Am. Chem. Soc.* **1993**, *115*, 6825−6834.

$^1J_{C1,C2}$, the changes are modest (2−3 Hz). Thus, present data on **3**−**5** suggest that $^1J_{C2,H2}$ in the biologically relevant monosaccharide, D-glucosamine, will be pH dependent, with larger couplings observed under acidic conditions. $^1J_{C2,H2}$ in D-glucopyranoses is also expected to be larger than $^1J_{C2,H2}$ in 2-amino-2-deoxy-D-glucopyranoses (free base) and smaller than $^1J_{C2,H2}$ in its corresponding hydrochloride salt. These predictions assume that the effects observed herein for glycosylamines are transferable to aminosugars having the amine substituent appended to non-anomeric carbons. The latter assumption, however, remains to be tested computationally.

These results have important implications for studies of trans-*O*-glycoside *J*-couplings in oligosaccharides. The C1−O4−C4−C5 coupling pathways in **3**−**5** bear resemblance to C−O−C−C coupling pathways across *O*-glycosidic linkages, and couplings across the latter pathways are useful conformational constraints in oligosaccharides.[31] The present results suggest that Karplus curves for O−C−C−O−C and N−C−C−O−C pathways should be similar; thus, for example, trans-*O*-glycoside couplings involving C2 of 2-aminosugars such as 2-acetamido-2-deoxy-*β*-D-glucopyranose might be expected to exhibit a dependence on torsion angle similar to that exhibited by *β*-D-glucopyranose. This prediction remains to be tested theoretically and experimentally with appropriate model structures and biologically relevant aminosugar-containing oligosaccharides, respectively.

(31) Bose, B.; Zhao, S.; Stenutz, R.; Cloran, F.; Bondo, P. B.; Bondo, G.; Hertz, B.; Carmichael, I.; Serianni, A. S. *J. Am. Chem. Soc.* **1998**, *120*, 11158−11173.